A LETTERS JOURNAL EXPLORING THE FRONTIERS OF PHYSICS

Società Italiana di Fisica

sciences IOP Institute of Physics

LETTER • OPEN ACCESS

Reentrant condensation transition in a model of driven scalar active matter with diffusivity edge

To cite this article: Jonas Berx *et al* 2023 *EPL* **142** 67004

View the article online for updates and enhancements.

You may also like

- Melting, reentrant ordering and peak effect for Wigner crystals with quenched and thermal disorder
C Reichhardt and C J O Reichhardt
- The 2020 motile active matter roadmap
Gerhard Gompper, Roland G Winkler, Thomas Speck et al.
- Effects of structural parameters on flow boiling performance of reentrant porous microchannels
Daxiang Deng, Yong Tang, Haoran Shao et al.

This content was downloaded from IP address 185.107.13.4 on 27/06/2023 at 08:20

A Letters Journal Exploring the Frontiers of Physics

June 2023

EPL, **142** (2023) 67004
doi: 10.1209/0295-5075/acdcb7

www.epljournal.org

Reentrant condensation transition in a model of driven scalar active matter with diffusivity edge

Jonas Berx[1,2], Aritra Bose[1], Ramin Golestanian[1,3] and Benoît Mahault[1(a)]

[1] *Max Planck Institute for Dynamics and Self-Organization (MPI-DS) - 37077 Gättingen, Germany*
[2] *Institute for Theoretical Physics, KU Leuven - B-3001 Leuven, Belgium*
[3] *Rudolf Peierls Centre for Theoretical Physics, University of Oxford - Oxford OX1 3PU, United Kingdom*

received 6 March 2023; accepted in final form 8 June 2023
published online 22 June 2023

Abstract – The effect of a diffusivity edge is studied in a system of scalar active matter confined by a periodic potential and driven by an externally applied force. We find that this system shows qualitatively distinct stationary regimes depending on the amplitude of the driving force with respect to the potential barrier. For small driving, the diffusivity edge induces a transition to a condensed phase analogous to the Bose–Einstein-like condensation reported for the nondriven case, which is characterized by a density-independent steady state current. Conversely, large external forces lead to a qualitatively different phase diagram since in this case condensation is only possible beyond a given density threshold, while the associated transition at higher densities is found to be reentrant.

open access Copyright © 2023 The author(s)

Published by the EPLA under the terms of the Creative Commons Attribution 4.0 International License (CC BY). Further distribution of this work must maintain attribution to the author(s) and the published article's title, journal citation, and DOI.

Introduction. – Systems for which detailed balance is broken at the microscopic scale are known as active matter [1]. This property endows them with the ability to exhibit collective behaviour impossible at equilibrium. Notable examples are the possibility of active particles to phase separate without attractive interactions [2–4], or to exhibit long-range orientational order in two dimensions [5–7].

In recent years, intensive efforts have been made to study the rich phenomenology of active systems via minimal models that capture their key features. Active particles are indeed routinely modelled as persistent walkers [8–11], and in a lattice gas setting as agents with an internal polarity setting a preferred hopping direction [12–15]. Without large-scale orientational order, the macroscopic dynamics of active systems is often captured by a nonlinear drift-diffusion equation describing the evolution of the particle density field [2,15–17]. Furthermore, because such equation describes a dynamics evolving far from equilibrium, its effective diffusivity and mobility *a priori* do not satisfy a Fluctuation Dissipation Relation (FDR) [18].

Due to the interplay between activity and particle interactions, some mean field active dynamics may be formulated in terms of an effective diffusivity that vanishes or becomes negative beyond a certain density threshold [2,19]. The class corresponding to a diffusivity remaining identically zero at large enough densities, which hereafter we will refer to as *diffusivity edge*, was introduced phenomenologically in [4]. There, it was shown that the coupling of the diffusivity edge with harmonic confinement triggers the formation of a point-like condensate at the ground state of the potential, while the corresponding transition exhibits remarkable similarities with Bose-Einstein Condensation (BEC) [20]. More recently, this BEC-like condensation transition was reported in numerical simulations of a model of magnetic microswimmers confined in a quasi-one-dimensional channel [19]. The BEC-like transition observed in the diffusivity edge class is furthermore reminiscent of condensation phenomena arising in various mass transport models [21–26].

In this work, we study the influence of an external driving on the behaviour of a scalar active matter system presenting a diffusivity edge. Working in one dimension, we achieve a nonvanishing steady state current by confining the dynamics in a tilted periodic potential. Due to

(a) E-mail: benoit.mahault@ds.mpg.de (corresponding author)

its generic nature, this setup plays a fundamental role in the modelling of a plethora of physical systems [27]. For example, it serves as a minimal model for active ratchets [28,29] at the origin of the rectification of the motion of microswimmers in asymmetric geometries [30,31] or the transport of asymmetric objects in active baths [32,33].

Although for weak external driving forces such that the potential has local minima the phenomenology of condensation resembles that observed at zero drive [34], the strong force regime where the potential is monotonous leads to striking differences. For strong forces our study indeed reveals the existence of a particle density threshold below which condensation cannot arise. The condensation transition at large enough densities, moreover, leads to the formation of a condensate occupying a finite volume, such that upon cooling the system may undergo a subsequent evaporation transition, leading to reentrance. All the theoretical results presented below are systematically compared to direct numerical simulations of the continuous theory governing the dynamics (details about numerical methods are given in the Supplementary Material `Supplementarymaterial.pdf` (SM)).

Scalar active matter with diffusivity edge. – We consider the following one-dimensional phenomenological evolution equation for a scalar density field $\rho(x,t)$:

$$\partial_t \rho + \partial_x J = 0, \qquad J = -M(\rho)\rho\partial_x U - D(\rho)\partial_x \rho, \quad (1)$$

where $U(x)$ is an externally applied potential, while $M(\rho)$, and $D(\rho)$ respectively denote the ρ-dependent effective mobility and diffusivity. When the microscopic dynamics satisfies detailed balance, the ratio between $M(\rho)$, and $D(\rho)$ obeys a FDR and is thus equal to the temperature of the system. With broken detailed balance, on the contrary, $D(\rho)/M(\rho)$ is not constrained by any FDR. A number of non-interacting active systems, however, satisfy a generalised FDR accounting for the renormalization of their effective diffusivity by activity [2,8,19,35]. Here, we therefore assume such a relation in the dilute limit, and define an effective temperature as

$$k_{\mathrm{B}}T_{\mathrm{eff}} \equiv \lim_{\rho\to 0} \frac{D(\rho)}{M(\rho)}, \quad (2)$$

which we will moreover use as a control parameter for the dynamics. For finite densities, due to the nonequilibrium character of active dynamics the ratio $D(\rho)/M(\rho)$ has *a priori* no reason to remain equal to $k_{\mathrm{B}}T_{\mathrm{eff}}$. In particular, here we impose a diffusivity edge beyond a threshold ρ_{c} such that $D(\rho)/M(\rho) = 0$ for $\rho \geq \rho_{\mathrm{c}}$.

When $U(x)$ is harmonic, such diffusivity edge induces the formation of a singular condensate at the ground state for T_{eff} below a transition temperature T_{c} [4]. Remarkably, although the dynamics described by eq. (1) is fully classical the corresponding condensation transition carries signatures of BEC. The BEC-like condensation moreover holds for periodic potentials presenting degenerate minima [34]. To investigate how the BEC-like condensation transition is modified by the presence of an external drive, we consider here the external potential $U(x) = V(x) - Fx$, whose periodic part $V(x)$ has a peak value V_{b} at $x = 0$ and satisfies $V(x+L) = V(x)$ with L denoting the period, while F is a stationary uniform driving force.

The steady state solution. – We now calculate the steady state solution of eq. (1), which satisfies $\partial_x J = 0$. For $F \neq 0$, it is thus associated with a non-vanishing uniform current $\bar{J}$. We moreover assume a constant mobility $M(\rho) = M_{\mathrm{s}}$, and a step diffusivity profile such that

$$D(\rho) = M_{\mathrm{s}} k_{\mathrm{B}} T_{\mathrm{eff}} \Theta(\rho_{\mathrm{c}} - \rho), \quad (3)$$

where Θ is the Heaviside step function. This simple way to implement the diffusivity edge, while it allows for analytical progress, does not qualitatively modify the properties of the condensation transition at $F = 0$ as compared to more realistic mobility and diffusivity profiles [4,34]. As we discuss in the final section, for $F \neq 0$ the properties of the system are also largely insensitive to the specific shape of $D(\rho)$. In what follows, we rescale space and time such that L and $M_{\mathrm{s}}V_{\mathrm{b}}$ are set to unity.

Assuming that the dynamics evolves on a ring, due to the translational invariance of the problem we express stationary density profiles over a single period of $V(x)$. With the above choice of parameters, we derive the steady state solution of eq. (1) via usual techniques [27] (see also the SM for calculation details). Defining $\beta \equiv (k_{\mathrm{B}}T_{\mathrm{eff}})^{-1}$ as the inverse effective temperature and assuming the density to be lower than ρ_{c} everywhere, we obtain

$$\rho(x) = \beta V_{\mathrm{b}} \bar{J} e^{-\beta U(x)} \left(\frac{I_+(1)}{1 - e^{-\beta F}} - I_+(x) \right), \quad (4)$$

with $I_+(x) \equiv \int_0^x \exp[\beta U(x')]\mathrm{d}x'$. The expression of the steady state current is then obtained from the normalization condition $\bar{\rho} = \int_0^1 \mathrm{d}x \rho(x)$, with $\bar{\rho}$ denoting the mean density in the system (see the SM).

Although the integrals in the expression of the steady state profile (4) can be numerically determined for an arbitrary periodic potential $V(x)$, it is instructive to consider the case of a sawtooth potential with anisotropy parameter $\alpha \in (0;1)$, such that

$$V(x) = V_{\mathrm{b}} \left(1 - \frac{x}{\alpha}\right) \times \begin{cases} 1, & 0 \leq x \leq \alpha, \\ \alpha/(\alpha - 1), & \alpha \leq x \leq 1, \end{cases} \quad (5)$$

and which is to be extended periodically with unit period. Note that with this choice the potential $U(x)$ is symmetric under the combined transformations $F \to -F$ and $\alpha \to 1 - \alpha$, such that we only consider positive values of F without loss of generality. The piecewise linearity of (5) conveniently leads to an exact expression for the density profile (4). Denoting ρ_0 as the maximum value of the density, we find that for $\rho_0 < \rho_{\mathrm{c}}$ the expression for the full

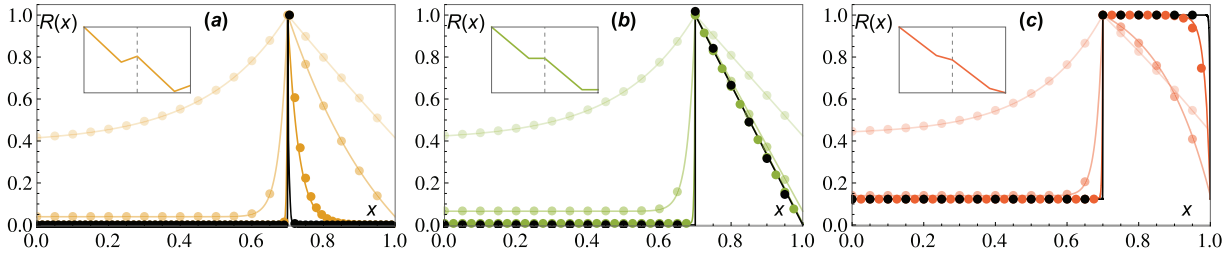

Fig. 1: Stationary density profiles, eq. (6), for $\alpha = \frac{7}{10}$ in the three regimes described in the text: panels (a), (b), (c) respectively correspond to $f = -0.7$, $f = 0$ and $f = 0.2$. Curves with increasing transparency correspond to an increase of the effective temperature $T_{\rm eff}$, while black lines correspond to $T_{\rm eff} \to 0$. In all panels dots indicate numerical simulation results, while solid lines correspond to the theoretical prediction. In each case the insets sketch two periods of $U(x)$ separated by a vertical dashed line.

profile can be recast as $\rho(x) = \rho_0 R(x)$ with

$$R(x) = \frac{1}{\gamma}\begin{cases} (1-e^{\beta V_{\rm b} f}) z^{\frac{x}{\alpha}} - \alpha f \left(z e^{\beta V_{\rm b} f} - 1\right), & 0 \le x \le \alpha, \\ (z-1)\, e^{\beta V_{\rm b} f \frac{x-\alpha}{1-\alpha}} & \\ -(1+\alpha f)(z e^{\beta V_{\rm b} f} - 1), & \alpha \le x \le 1, \end{cases} \tag{6}$$

where we have defined the dimensionless force $f \equiv F/F_{\rm c} - 1$ with $F_{\rm c} \equiv V_{\rm b}/(1-\alpha)$, and

$$z \equiv e^{\frac{\beta V_{\rm b}(1+\alpha f)}{1-\alpha}}, \quad \gamma \equiv z\left(1 - e^{\beta V_{\rm b} f}\right) - \alpha f \left(z e^{\beta V_{\rm b} f} - 1\right).$$

ρ_0 can moreover be expressed in terms of the steady state current $\bar{J}$, which yields

$$\rho_0 = \frac{\bar{J}(1-\alpha)}{f(1+\alpha f)}\left(\alpha f + \frac{z(1-e^{\beta V_{\rm b} f})}{1 - z e^{\beta V_{\rm b} f}}\right). \tag{7}$$

Looking back at the expression of the potential (5), it is clear that $F_{\rm c}$ corresponds to the value of the external forcing such that the full potential U becomes monotonous. In the following, we thus distinguish between the dynamical regimes associated with $f < 0$ ($F < F_{\rm c}$) and $f > 0$ ($F > F_{\rm c}$), which we will respectively refer to as subcritical and supercritical. As shown in fig. 1, the solution (6) in the subcritical regime consists of two convex branches decaying from ρ_0 at $x = \alpha$. For $f = 0$, on the contrary, due to the vanishing potential slope in the range $\alpha \le x \le 1$ the corresponding branch decays linearly from ρ_0, while in the supercritical regime it takes a concave shape. The maximum value of the density, ρ_0, typically increases with $\beta V_{\rm b}$ and $\bar{\rho}$, while it decreases with increasing f. In the limit $\beta V_{\rm b} \gg 1$ of small effective temperatures the expression of ρ_0 moreover simplifies as

$$\rho_0 \underset{\beta V_{\rm b} \gg 1}{\sim} \frac{\bar{\rho}}{1-\alpha}\begin{cases} -\beta V_{\rm b} f(1+\alpha f) & (f < 0), \\ 2 & (f = 0), \\ \dfrac{(1-\alpha)(1+\alpha f)}{1+\alpha(f-1)} & (f > 0), \end{cases} \tag{8}$$

while for large effective temperatures fluctuations dominate over the confinement, such that the density profile is nearly uniform and $\rho_0 \sim \bar{\rho}$ for $\beta V_{\rm b} \ll 1$ and for all f.

The solution (6), however, holds only so long as ρ_0 remains below the diffusivity edge $\rho_{\rm c}$. When $\rho_0 = \rho_{\rm c}$, the stationary density profile becomes singular at $x = \alpha$ which reflects the fact that the system undergoes a condensation transition [4]. Using (7) and calculating $\bar{J}$ from the normalization of ρ, we find that the corresponding condition on the parameters $\bar{\rho}/\rho_{\rm c}$, $\beta V_{\rm b}$, α and f reads

$$\frac{\bar{\rho}}{\rho_{\rm c}} = \frac{(z e^{\beta V_{\rm b} f} - 1)(1 + \alpha(f-1)) - \frac{(1-\alpha)(z-1)(e^{\beta V_{\rm b} f} - 1)}{\beta V_{\rm b} f (1+\alpha f)}}{z(e^{\beta V_{\rm b} f} - 1) + \alpha f (z e^{\beta V_{\rm b} f} - 1)}. \tag{9}$$

We now analyse the properties of the transition and the nature of the condensate and discuss how they are affected by the presence of a nonzero driving force. From now on we fix $\alpha = \frac{7}{10}$ for all numerical evaluations. In all figures theoretical results are displayed with solid lines while numerical data from simulations of eq. (1) are shown with symbols.

The subcritical regime. – For $f < 0$ the potential $U(x)$ exhibits a local minimum at $x = \alpha$. This case is therefore qualitatively similar to the nondriven case addressed in ref. [34]. The transition lines obtained from (9) at fixed f and $\bar{\rho}$ are shown respectively in fig. 2(a), (b) (see the blue and yellow curves). They predict the existence of a transition for all $\bar{\rho} < \rho_{\rm c}$, while the transition temperature in the limit of vanishing densities reads

$$\frac{k_{\rm B} T_{\rm c}}{V_{\rm b}} \underset{\bar{\rho} \ll \rho_{\rm c}}{\sim} -\frac{\bar{\rho}}{\rho_{\rm c}} \frac{f(1+\alpha f)}{1-\alpha}. \tag{10}$$

For $T_{\rm eff} < T_{\rm c}$, the density profile in the condensed phase can moreover formally be written as

$$\rho(x) = \bar{\rho}\phi_{\rm c}\delta(x-\alpha) + \rho_{\rm c} R(x) \qquad (T_{\rm eff} < T_{\rm c}), \tag{11}$$

with the function $R(x)$ defined in eq. (6). This solution thus consists of a smooth part with maximum density given by $\rho_{\rm c}$ and a singular condensate located at the local potential minimum $x = \alpha$. The condensate fraction, $\phi_{\rm c}$, is then determined from the density normalization. The expression of $\phi_{\rm c}$ in the general case is rather lengthy and does not yield much physical insight, but taking the limits

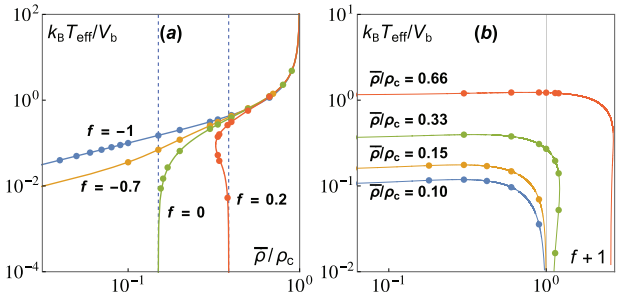

Fig. 2: Phase diagrams computed from the condition (9), showing the effective transition temperature as a function of mean density $\bar{\rho}$ at fixed f (a) or as a function of f at fixed $\bar{\rho}$ (b). In panel (a) the two vertical dashed lines mark the density ratio λ (cfr. eq. (15)) below which no condensation occurs in the limit $T_{\rm eff} \to 0$.

of small and large effective temperatures it simplifies as

$$\phi_c \underset{\beta V_b \gg 1}{\sim} 1 - \frac{T_{\rm eff}}{T_c}, \quad \phi_c \underset{\beta V_b \ll 1}{\sim} \left(1 - \frac{\rho_c}{\bar{\rho}}\right)\left(1 - \frac{T_c}{T_{\rm eff}}\right). \tag{12}$$

These expressions correspond to those derived in [34], and match well with the full solution in the low temperature regime (fig. 3(a)). The presence of a weak driving force thus does not qualitatively modify the scaling of the condensate fraction with effective temperature but only affects the value of the transition temperature T_c.

Since the condensate is located at a local minimum of the potential, it does not contribute to the global current $\bar{J}$. Therefore, the latter is obtained from eq. (7) by replacing ρ_0 with ρ_c, namely

$$\bar{J} = \frac{\rho_c f(1+\alpha f)}{(1-\alpha)}\left(\alpha f + \frac{z(1-e^{\beta V_b f})}{1 - z e^{\beta V_b f}}\right)^{-1} \qquad (T_{\rm eff} < T_c). \tag{13}$$

Remarkably, $\bar{J}$ does not depend on the mean particle density $\bar{\rho}$, which reflects the fact that increasing $\bar{\rho}$ does not affect the smooth part of the distribution (11) (cfr. inset of fig. 3(b)), but only leads to an increase of the condensate fraction ϕ_c. This feature is analogous to the divergence of the isothermal compressibility at $T_{\rm eff} = T_c$ found in the nondriven case [4,34], which implies that the confining pressure exerted by the potential is independent of $\bar{\rho}$.

The BEC-like condensation transition at $F = 0$ is moreover associated with a singular behaviour of several observables such as the mean internal energy $\langle U \rangle \equiv \int_0^1 \mathrm{d}x \rho(x) U(x)$ or the heat capacity $C \equiv \mathrm{d}\langle U \rangle / \mathrm{d}T_{\rm eff}$ [4]. For $F > 0$, the explicit expressions of these thermodynamic functions, although they can straightforwardly be obtained from eq. (6), are generally quite lengthy and we do not report them here. Some asymptotic results are given in the SM. Figure 3(c), (d) shows that their behavior at the transition is qualitatively similar to the nondriven case, with $\langle U \rangle$ exhibiting a discontinuous slope at $T_{\rm eff} = T_c$, resulting in a discontinuous jump of C. In addition, in the limit of strong confinement, the mean particle

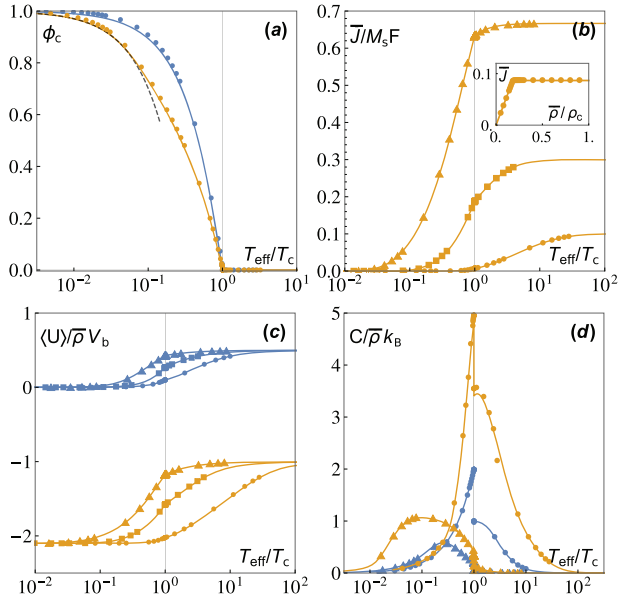

Fig. 3: Subcritical ($f < 0$) condensation transition with $f = -1$ (blue) and $f = -0.7$ (orange). (a) Condensate fraction ϕ_c for $\bar{\rho}/\rho_c = 0.33$ (the black dashed line shows the low temperature approximation (12)). (b)–(d) Stationary current $\bar{J}$ (b), mean internal energy (c) and heat capacity (d) as a function of $T_{\rm eff}$. The inset in (b) shows $\bar{J}$ *vs.* $\bar{\rho}$ at fixed $T_{\rm eff} = 0.1$, condensation occurs at $\bar{\rho}/\rho_c \approx 0.19$. Dots, squares and triangles respectively correspond to $\bar{\rho}/\rho_c = 0.1$, 0.3 and 0.66.

current can be expressed as

$$\bar{J} \underset{\beta V_b \gg 1}{\sim} -\frac{\rho_c f(1+\alpha f)}{1-\alpha} e^{-\frac{1-\alpha}{1+\alpha f}\frac{\rho_c}{\bar{\rho}}\frac{T_c}{T_{\rm eff}}} \begin{cases} \dfrac{T_c}{T_{\rm eff}} & (T_{\rm eff} \geq T_c), \\ 1 & (T_{\rm eff} < T_c), \end{cases} \tag{14}$$

which highlights that the condensation transition is associated with a cusp in the decay of $\bar{J}$ with the effective temperature (fig. 3(b)). Finally, eq. (14) also indicates that the presence of a condensate leads to a faster decay of the current with the effective temperature.

The supercritical regime. – We now address the case $f \geq 0$, which marks a qualitative change in the phase diagram of the system (see the green and red curves in fig. 2). Indeed, it appears from eq. (8) that for $f \geq 0$ the condensed phase can be reached at zero effective temperature only for $\bar{\rho} \geq \lambda \rho_c$ with

$$\lambda \equiv \begin{cases} (1-\alpha)/2 & (f = 0), \\ (1 - \alpha + \alpha f)/(1 + \alpha f) & (f > 0). \end{cases} \tag{15}$$

Taking $f = 0$, numerical simulations of eq. (1) reveal that the condensate remains point-like (fig. 4(a)). Therefore, density profiles in the condensed phase are described by eq. (11). This case is thus analogous to the subcritical regime, with however some qualitative differences in the low effective temperature limit. Taking $f = 0$ and

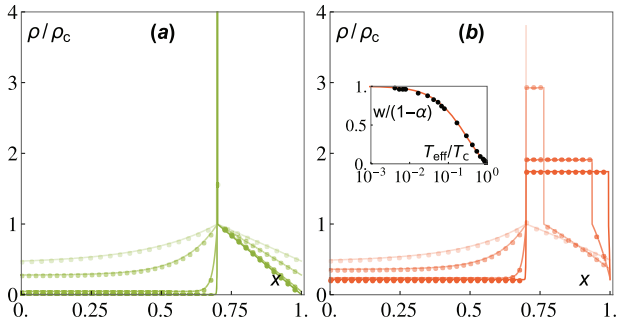

Fig. 4: Condensed density profiles for $f = 0$ (a) and $f = 0.2$ (b) at fixed $\bar{\rho}/\rho_c = 2/3$ for various effective temperatures. Curves with increasing opacity correspond to decreasing $T_{\rm eff}$. In (a) the point-like condensate density is truncated for clarity. The inset in (b) shows how the condensate width varies with $T_{\rm eff}$.

$\beta V_b \gg 1$ in eq. (13), we find that the current vanishes linearly with the effective temperature,

$$\bar{J} \underset{T_{\rm eff}\to 0}{\sim} \frac{\rho_c}{1-\alpha}\frac{k_B T_{\rm eff}}{V_b} \qquad (T_{\rm eff} < T_c, f = 0),$$

in contrast with the faster exponential decay found in the subcritical regime (see eq. (14)). Correspondingly, we find that in the limit of zero effective temperature the condensate does not contain all the mass of the system but carries a finite fraction equal to $\phi_c \underset{T_{\rm eff}\to 0}{\sim} 1 - \lambda\rho_c/\bar{\rho}$. This feature can be explained by the fact that, since for $f = 0$ the potential is no more confining, it allows for spatial coexistence between a point-wise condensate at $x = \alpha$ and a residual gas phase even for $T_{\rm eff} = 0$. Figure 4(a) shows that this gas phase is indeed located in the region where the net force balances to zero, and hence can persist even for $T_{\rm eff} = 0$ without inducing a global current.

Considering now the supercritical regime at $f > 0$, we find from numerical simulations of eq. (1) that the condensate is only point-like at $T_{\rm eff} = T_c$, while for $T_{\rm eff} < T_c$ it consists of a uniform domain of finite density extending from $x = \alpha$ with a width w (fig. 4(b)). Therefore, $f = 0$ marks a depinning transition from a point-wise condensate to an extended condensate occupying a finite volume. Consequently, for $f > 0$ cooling down the system from T_c may result in the condensate density becoming lower than ρ_c at $T_{\rm eff} \equiv T_e < T_c$, leading to a low-temperature evaporation transition. We find that such a scenario typically occurs for $\bar{\rho} \lesssim \lambda\rho_c$, and therefore that in the supercritical regime the transition to condensation is reentrant, as shown in the phase diagrams of fig. 2. In the SM we moreover provide a theoretical argument for the supercritical reentrant transition in the low effective temperature limit. Reentrant condensation transitions have been observed in models of two-species zero-range processes [36], while in the context of active matter reentrance was also predicted for motility induced phase separation [37].

To study the condensed phase at $f > 0$, we describe the density profile as a piecewise function defined on the three intervals $[0;\alpha]$, $[\alpha;x^*]$ and $[x^*;1]$ with $x^* \equiv \alpha + w$. Solving eq. (1) for a steady state with constant current $\bar{J}$ for $x \le \alpha$ and $x^* \le x$, while assuming a uniform condensate of density $\bar{\rho}\phi_c/w > \rho_c$ in between, we obtain

$$\rho(x) \underset{f>0}{=} \begin{cases} \dfrac{\bar{J}\alpha(1-\alpha)}{1+\alpha f}\left(1 - z^{\frac{x}{\alpha}-1}\right) + \rho_c z^{\frac{x}{\alpha}-1}, & 0 \le x \le \alpha, \\ \bar{\rho}\phi_c/w, & \alpha < x < x^*, \\ \dfrac{\bar{J}(1-\alpha)}{f}\left(1 - e^{\beta V_b f \frac{x-x^*}{1-\alpha}}\right) & \\ \quad + \rho_c e^{\beta V_b f \frac{x-x^*}{1-\alpha}}, & x^* \le x \le 1, \end{cases} \tag{16}$$

where we have used the fact that $\rho(\alpha) = \rho(x^*) = \rho_c$. The periodicity condition $\rho(0) = \rho(1)$ then allows to express the condensate width w as a function of the current $\bar{J}$. Finally, a closed expression for the current is obtained from $\bar{J} = -V_b^{-1}\int_0^1 {\rm d}x U'(x)\rho(x)$ which, after eliminating ϕ_c, leads to (details in the SM)

$$\bar{J} \underset{f>0}{=} \frac{\rho_c(1+\alpha f)}{\kappa}\left[1 - \frac{1}{z} + \frac{\beta V_b f(1+\alpha f)}{1-\alpha}\frac{\bar{\rho}}{\rho_c}\right] \qquad (T_{\rm eff} < T_c), \tag{17}$$

where $\kappa \equiv \alpha(1-\alpha)(1-z^{-1}) + \lambda\beta V_b(1+\alpha f)^2$.

Since for $f > 0$ the condensate occupies a finite volume, it contributes to the global current that now explicitly depends on the mean particle density, in contrast with eq. (13) derived in the subcritical regime. Equation (17) can then be used to calculate the condensate width w as well as the condensate fraction ϕ_c in the SM. Close to the transition, we find that both expressions simplify as

$$w \underset{T_{\rm eff}\lesssim T_c}{\propto} \frac{T_c}{T_{\rm eff}} - 1, \qquad \phi_c \underset{T_{\rm eff}\lesssim T_c}{\propto} 1 - \frac{T_{\rm eff}}{T_c} \qquad (f > 0),$$

such that near the threshold the condensate density decays linearly with the effective temperature: $\bar{\rho}\phi_c/w \propto T_{\rm eff}/T_c$.

In the condensed phase, we moreover find that the solution (16) matches perfectly with the profiles obtained from numerical simulations of eq. (1) (fig. 4(b)). Furthermore, the thermodynamics of condensation carries the BEC signatures similarly to the subcritical regime (fig. 5). The current and mean energy indeed exhibit a discontinuous slope at $T_{\rm eff} = T_c$ associated with a discontinuous jump of the heat capacity. Remarkably, in the reentrant regime these features also hold for the evaporation transition at $T_{\rm eff} = T_e$, despite the condensate not being point-like in this case.

In the limit of small effective temperatures, we find that the condensate width approaches $1 - \alpha$ from below as

$$1 - \alpha - w \underset{T_{\rm eff}\to 0}{\propto} \frac{T_{\rm eff}}{T_c} \qquad (f > 0),$$

while the current and condensate fraction converge to

$$\bar{J} \underset{T_{\rm eff}\to 0}{\sim} \frac{\bar{\rho} f}{(1-\alpha)\lambda}, \quad \phi_c \underset{T_{\rm eff}\to 0}{\sim} 1 - \frac{\alpha^2 f}{(1+\alpha f)\lambda}, \quad (f > 0).$$

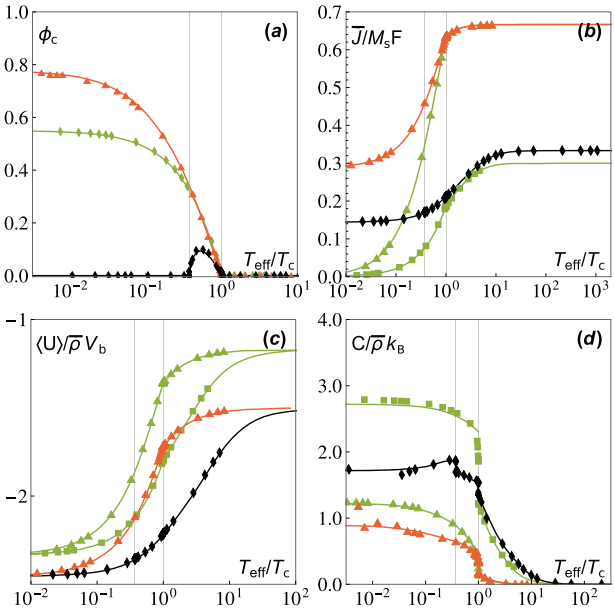

Fig. 5: Transition to condensation in the supercritical regime ($f \geq 0$), with $f = 0$ (green) and $f = 0.2$ (red and black, respectively corresponding to the regimes without and with reentrance). Squares, diamonds and triangles respectively correspond to $\bar{\rho}/\rho_{\rm c} = 0.3$, 0.33 and 0.66. Vertical lines indicate the condensation and evaporation (happening only for the data shown in black) thresholds $T_{\rm c}$ and $T_{\rm e}$.

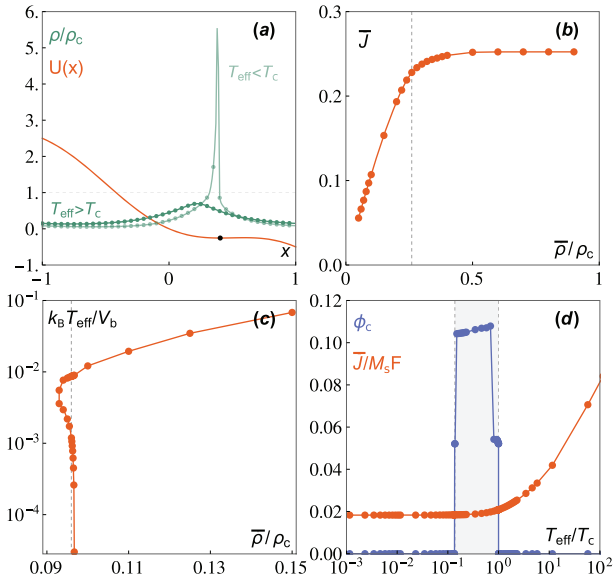

Fig. 6: Condensation transition in a sinusoidal potential with $V_{\rm b} = 1$. (a) Density profiles for $T_{\rm eff} > T_{\rm c}$ and $T_{\rm eff} < T_{\rm c}$ with $f = -0.05$. The potential is also shown with its minimum (black dot). (b) Scaling of $\bar{J}$ with the mean density while crossing the transition at $\bar{\rho}/\rho_{\rm c} \approx 0.26$ at fixed $T_{\rm eff} = 0.5$. (c) Phase diagram showing $T_{\rm c}$ as a function of $\bar{\rho}$. (d) Current and condensate fraction as a function of $T_{\rm eff}$ at $\bar{\rho}/\rho_{\rm c} \approx 0.096$ and $f \approx 0.02$. Here lines are drawn as a guide for the eye.

As a consequence of the depinning transition, in the supercritical regime the current saturates to finite values for $T_{\rm eff} = 0$. Similarly to the $f = 0$ case, the condensate fraction moreover saturates to a finite value, which highlights a gas-condensate coexistence. Indeed, the density distribution at $T_{\rm eff} = 0$ and $f > 0$ simply consists of two disconnected plateaus with respective values

$$\rho(x) \underset{T_{\rm eff}\to 0}{\sim} \frac{\bar{\rho}}{\lambda} \begin{cases} \alpha f/(1+\alpha f), & 0 \leq x \leq \alpha \\ 1, & \alpha < x \leq 1 \end{cases} \qquad (f > 0).$$

Generalization to the sinusoidal potential. – All the results obtained so far correspond to the step diffusivity profile (3) and the sawtooth periodic potential (5), which allow for exact derivations. To assess their generality, we now consider a different setting for which the diffusivity edge is reached as (keeping the previous notations)

$$D(\rho) = M_{\rm s} k_{\rm B} T_{\rm eff} (1 - \rho/\rho_{\rm c})^2 \, \Theta(\rho_{\rm c} - \rho), \qquad (18)$$

while the periodic potential is sinusoidal: $V(x) = \frac{V_{\rm b}}{2}[1 - \cos(\pi x)]$. As expected, this choice leads to density profiles smoother than obtained previously with the sawtooth potential (fig. 6(a)). Looking at the condition for the full potential to be monotonous, the threshold associated with the depinning transition is in this case $F_{\rm c} = \pi V_{\rm b}/2$.

In the subcritical regime for which $f = F/F_{\rm c} - 1 \leq 0$, numerical simulations of eq. (1) reveal that the phenomenology of the transition is similar to that described previously. Given a mean particle density $\bar{\rho} < \rho_{\rm c}$ and a driving force $f < 0$, there always exists a value $T_{\rm c} > 0$ of $T_{\rm eff}$ such that the maximum density reaches $\rho_{\rm c}$ and the system condenses. In this case, however, the maximum of the density profile (4) is distinct from the local minimum of the total potential $U(x)$ (fig. 6(a)). Therefore, the condensate is generally not point-like but has a finite width. Consequently, the condensate contributes to the current $\bar{J}$ which increases sub-linearly with the mean particle density for $T_{\rm eff} < T_{\rm c}$ (fig. 6(b)). The condensate width, however, is in general fairly small and converges to zero as $T_{\rm eff} \to 0$, such that its effect on $\bar{J}$ is hardly appreciable in numerical simulations.

Taking now $f > 0$, similarly to what was described previously for the sawtooth potential there exists a finite density threshold below which no condensation occurs (fig. 6(c)). Noting that the supercritical regime is defined as when the potential becomes strictly monotonous, the zero-temperature density profile indeed obeys in steady state (assuming that U is smooth) $\bar{J} = -\rho(x)U'(x)$ such that, after using the normalization condition,

$$\rho(x) \underset{f>0}{=} \bar{\rho} \left[U'(x) \int_0^1 \frac{{\rm d}y}{U'(y)} \right]^{-1} \qquad (T_{\rm eff} = 0). \qquad (19)$$

Hence, we deduce that in the limit of vanishing effective temperatures condensation only happens for $\bar{\rho} \geq \lambda \rho_{\rm c}$ with

$$\lambda = \min_x [|U'(x)|] \int_0^1 \frac{{\rm d}y}{|U'(y)|}. \qquad (20)$$

For the sinusoidal potential, we find $\lambda = \sqrt{f/(2+f)}$ which is in agreement with our numerical simulations (fig. 6(c)). More remarkably, our numerical results point towards a reentrant transition with the system undergoing an evaporation transition at $T_{\rm eff} = T_{\rm e} < T_{\rm c}$, highlighting the generality of this feature (figs. 6(c), (d)).

Conclusion. – We have studied the effect of nonzero steady state currents on the BEC-like condensation induced by a diffusivity edge. In contrast with the nondriven case, the condensate at nonzero drive might occupy a finite volume similar to what was observed in mass transport models with finite-range interactions [22,23]. Moreover, the stationary current is found to be essentially independent of the mean particle density in the condensed phase of subcritical regime, a feature that has also been described for the externally driven zero-range process [38]. The most prominent differences with respect to previous studies of the diffusivity edge class were observed in the supercritical regime. There, we found that condensation can only occur beyond a minimum particle density, while the corresponding transition is reentrant at moderate densities due to the presence of an evaporation transition at low effective temperatures.

The results presented here highlight the similarities between the diffusivity edge class and a variety of mass transport models. Characterising further these similarities at the dynamical level, *e.g.*, to study the coarsening of the condensate or to investigate the presence of kinematic waves such as those observed in the zero-range process [38], requires to go beyond the mean field level considered here. Introducing noise in the dynamics would moreover allow to study the interplay between other features of externally driven Brownian motion, such as the enhanced effective diffusion [39,40], with the BEC-like condensation.

* * *

This work has received support from the Max Planck School Matter to Life and the MaxSynBio Consortium, which are jointly funded by the Federal Ministry of Education and Research (BMBF) of Germany, and the Max Planck Society.

Data availability statement: All data that support the findings of this study are included within the article (and any supplementary files).

REFERENCES

[1] Gompper G. *et al.*, *J. Phys.: Condens. Matter*, **32** (2020) 193001.
[2] Cates M. E. and Tailleur J., *Annu. Rev. Condens. Matter Phys.*, **6** (2015) 219.
[3] Cotton M. W. *et al.*, *Phys. Rev. Lett.*, **129** (2022) 158101.
[4] Golestanian R., *Phys. Rev. E*, **100** (2019) 010601(R).
[5] Toner J. and Tu Y., *Phys. Rev. Lett.*, **75** (1995) 4326.
[6] Chaté H., *Annu. Rev. Condens. Matter Phys.*, **11** (2020) 189.
[7] Mahault B. and Chaté H., *Phys. Rev. Lett.*, **127** (2021) 048003.
[8] Romanczuk P. *et al.*, *Eur. Phys. J. ST*, **202** (2012) 1.
[9] Howse J. R. *et al.*, *Phys. Rev. Lett.*, **99** (2007) 048102.
[10] Bechinger C. *et al.*, *Rev. Mod. Phys.*, **88** (2016) 045006.
[11] Zöttl A. and Stark H., *J. Phys.: Condens. Matter*, **28** (2016) 253001.
[12] Thompson A. G. *et al.*, *J. Stat. Mech.: Theory Exp.*, **2011** (2011) P02029.
[13] Solon A. P. and Tailleur J., *Phys. Rev. Lett.*, **111** (2013) 078101.
[14] Soto R. and Golestanian R., *Phys. Rev. E*, **89** (2014) 012706.
[15] Kourbane-Houssene M. *et al.*, *Phys. Rev. Lett.*, **120** (2018) 268003.
[16] Chavanis P. H., *Eur. Phys. J. B: Condens. Matter*, **62** (2008) 179.
[17] Chakraborty T. *et al.*, *Phys. Rev. E*, **101** (2020) 052611.
[18] Kubo R., *Rep. Prog. Phys.*, **29** (1966) 255.
[19] Meng F. *et al.*, *Phys. Rev. Lett.*, **126** (2021) 078001.
[20] Ziff R. M. *et al.*, *Phys. Rep.*, **32** (1977) 169.
[21] Evans M. R. and Hanney T., *J. Phys. A: Math. Theor.*, **38** (2005) R195.
[22] Evans M. R. *et al.*, *Phys. Rev. Lett.*, **97** (2006) 010602.
[23] Evans M. R. and Waclaw B., *J. Phys. A: Math. Theor.*, **47** (2014) 095001.
[24] Majumdar S. N. *et al.*, *Phys. Rev. Lett.*, **81** (1998) 3691.
[25] Majumdar S. N. *et al.*, *J. Stat. Phys.*, **99** (2000) 1.
[26] Chakraborti S. *et al.*, *Phys. Rev. E*, **103** (2021) 042133.
[27] Risken H., *The Fokker-Planck Equation*, 2nd edition (Springer, Berlin) 1996.
[28] Angelani L. *et al.*, *EPL*, **96** (2011) 68002.
[29] Reichhardt C. O. and Reichhardt C., *Annu. Rev. Condens. Matter Phys.*, **8** (2017) 51.
[30] Galajda P. *et al.*, *J. Bacteriol.*, **189** (2007) 8704.
[31] Leonardo R. D. *et al.*, *Proc. Natl. Acad. Sci. U.S.A.*, **107** (2010) 9541.
[32] Kaiser A., Peshkov A. *et al.*, *Phys. Rev. Lett.*, **112** (2014) 158101.
[33] Mallory S. A. *et al.*, *Phys. Rev. E*, **90** (2014) 032309.
[34] Mahault B. and Golestanian R., *New J. Phys.*, **22** (2020) 063045.
[35] Loi D. *et al.*, *Phys. Rev. E*, **77** (2008) 051111.
[36] Daga B., *Physica A*, **477** (2017) 1.
[37] Paoluzzi M. *et al.*, *Phys. Rev. Res.*, **2** (2020) 023207.
[38] Schütz G. M. and Harris R. J., *J. Stat. Phys.*, **127** (2007) 419.
[39] Reimann P. *et al.*, *Phys. Rev. Lett.*, **87** (2001) 010602.
[40] Reimann P., *Phys. Rep.*, **361** (2002) 57.